

Review Article

Biocidal Silver and Silver/Titania Composite Films Grown by Chemical Vapour Deposition

D. W. Sheel, L. A. Brook, I. B. Ditta, P. Evans, H. A. Foster, A. Steele, and H. M. Yates

Institute for Materials Research, Salford University, Manchester, M5 4WT, UK

Correspondence should be addressed to D. W. Sheel, d.w.sheel@salford.ac.uk

Received 27 March 2008; Revised 27 March 2008; Accepted 19 May 2008

Recommended by Russell Howe

This paper describes the growth and testing of highly active biocidal films based on photocatalytically active films of TiO₂, grown by thermal CVD, functionally and structurally modified by deposition of nanostructured silver via a novel flame assisted combination CVD process. The resulting composite films are shown to be highly durable, highly photocatalytically active and are also shown to possess strong antibacterial behaviour. The deposition control, arising from the described approach, offers the potential to control the film nanostructure, which is proposed to be crucial in determining the photo and bioactivity of the combined film structure, and the transparency of the composite films. Furthermore, we show that the resultant films are active to a range of organisms, including Gram-negative and Gram-positive bacteria, and viruses. The very high-biocidal activity is above that expected from the concentrations of silver present, and this is discussed in terms of nanostructure of the titania/silver surface. These properties are especially significant when combined with the well-known durability of CVD deposited thin films, offering new opportunities for enhanced application in areas where biocidal surface functionality is sought.

Copyright © 2008 D. W. Sheel et al. This is an open access article distributed under the Creative Commons Attribution License, which permits unrestricted use, distribution, and reproduction in any medium, provided the original work is properly cited.

1. INTRODUCTION

In recent years, TiO₂ has been widely investigated for its interesting photoexcited properties, for example, using photocatalysis can lead to the decomposition of organics into harmless products under UV light irradiation [1]. The extent of the photoactivity depends on a wide range of properties including morphology, crystallinity, and surface area.

The use of TiO₂ as a biocide was first demonstrated by Matsunaga et al. (1985) [2]. Subsequently, there have been a number of reports of disinfection of bacteria, viruses, and other micro-organisms. Most of this early work [3] used suspensions of TiO₂ and planktonic organisms. More recently, research has examined the interaction of organisms with biocidal thin films of TiO₂ anchored to solid surfaces [4–7]. Maness et al. have suggested that the mechanism by which titania is able to kill bacteria involves the disruption of the cell membrane following peroxidation of the membrane lipids by active oxygen species [3]. This is supported by the work of Sunada et al. [8] who studied killing of *Escherichia coli* on thin Cu/TiO₂ films and showed that firstly, the outer membrane was damaged followed by the

cytoplasmic membrane and that these processes then allowed the complete degradation of the cells. Amézaga-Madrid et al. [9] studied the inactivation of *Pseudomonas aeruginosa* and showed cell damage consistent with membrane and cell-wall damage.

Bulk Ag has been long used for coating many items including mirrors (for reflectance properties) and electrical contacts, as it is the most conductive of all metals. There is particular interest in nanoparticulate Ag due to its ability to act as both an electron sink and as redox catalyst. The antimicrobial properties of silver were well known to the ancient Egyptians and Greeks, for example, Hippocrates mentions silver as a treatment for ulcers [10]. Since then silver has been widely used as an antimicrobial agent in applications such as wound dressings and as surface coatings, for example, catheters [11, 12]. Silver has also been incorporated into bioglass [13]. Silver ions (Ag⁺) interact strongly with electron donors, and the antimicrobial activity of Ag primarily involves interactions with sulphhydryl groups in proteins [14–17]. Silver also reacts with other cellular components such as nucleic acids [18]. Silver has been shown to inhibit energy production by inhibition of the respiratory

chain of *Escherichia coli* [19]. Indirect toxicity may also arise from salt formation with silver ions that results in a chloride or anion limitation within the cell. Nanocrystalline silver [20] also releases Ag^0 and has been shown to rapidly kill bacteria and fungi [21]. Although Ag^+ is rapidly inactivated by interaction with organic matter, Ag^0 is much more stable [22].

The combination of Ag and TiO_2 for catalysis has been much studied for mainly sol-gel produced materials [23–25] with some colloid production of mixed [26] and core-shell composite clusters [27]. Most of these papers conclude that Ag is capable, under the correct conditions, of improving TiO_2 photoactivity. The addition of Ag promotes the charge separation of the electron-hole pairs from TiO_2 after photon absorption by acting as an electron sink. Also the plasmon resonance in metallic Ag nanoparticles is considered to locally enhance the electric field facilitating electron-hole production [28]. While most relate this improvement to electronic effects, it has been pointed out that the addition of Ag can modify the grain sizes of the TiO_2 , so increasing the surface area and hence also the photoactivity [24].

FACVD is a low-cost relatively simple atmospheric pressure CVD technique that is compatible with small volume, batch, and high volume continuous coating processes. A flame is used to provide the energy required to crack the precursor species into fragments and subsequently forms the film upon the substrate. Use of this method with low hazard aqueous solutions of simple metal salts can yield thin films, which represents a major advantage in terms of precursor cost and environmental impact compared to alternative CVD methods. In a previous paper [29], we also reported the use of aerosol delivery of aqueous solutions of silver salts in combination with FACVD, overcoming the previous limitations that atmospheric pressure CVD growth requires precursors with moderately high-vapour pressures. In this publication, we reported the first use of FACVD for silver deposition in combination with titania. We showed that this composite had biocidal activity toward (gram negative) *Escherichia coli*.

In this paper, we have now extended the work to explore a wider range of films structures, demonstrate significantly enhanced activity levels, and widen the exploration of biocidal activity to include gram positive bacteria (*Staphylococcus epidermidis*), and a virus (bacteriophage).

2. EXPERIMENTAL

2.1. Growth

All films were grown on pre-coated (CVD) silica coated barrier glass substrates. The barrier was a (60 nm) amorphous film of SiO_2 designed to prevent diffusion of impurity ions within the float glass. These would all cause a reduction in the quality and photoactivity of the films. All TiO_2 films used for biocidal testing were grown using an atmospheric pressure CVD coater described previously [30]. The precursor used was titanium tetra-isopropoxide ($7.79 \times 10^{-4} \text{ mol min}^{-1}$) (TTIP from Sigma-Aldrich, Mo, USA), which was trans-

ported through the reactor by a carrier gas of nitrogen. The substrate temperature was 500°C for TTIP.

Additionally, some films were grown using TiCl_4 and ethyl acetate at a substrate temperature of 650°C , for comparison purposes. The Ag films were grown using an atmospheric pressure flame assisted CVD coater with a propane/oxygen flame, described in detail previously [31]. The substrate temperature was set at 300°C . An aqueous solution of 0.5 M AgNO_3 was nebulised, into a carrier of N_2 , through the flame and onto the substrate.

2.2. Characterisation

Standard techniques of X-ray diffraction (Siemens D5000, Surrey, UK), micro-Raman 514.5 nm Ar line (Renishaw 1000, Gloucestershire, UK), UV/visible spectroscopy (Hewlett Packard HP895A, Bracknell, UK), and SEM (Philips XL30, Surrey, UK, equipped with a Rontec Quantax silicon drift diode detector 3rd generation (SDD3) energy dispersive X-ray spectrometer (EDAX)) were used to characterise the samples. Film thickness was estimated by relating the reflected colour to a calibrated chart for thickness versus refractive index. X-ray photoelectron spectroscopy, XPS, (Kratos AXIS Ultra, Calif, USA) with an Al (monochromated) K_α radiation source was used to check the surface characteristics of the films. It was necessary to use a charge neutraliser as all the samples were insulating, due mainly to the deposition on glass. This tends to shift the peak positions up to 2 eV so the measurements are referenced to the residual C 1s signal at 285 eV. Curve fitting used CASA XP software using a mixture of Gaussian-Lorentzian functions to deconvolute spectra.

To test the functional behaviour of the samples, both photoactivity and bioactivity were tested.

2.2.1. Photocatalytic behaviour

This was measured under UV (365 nm) at 20°C under open laboratory conditions. The emission spectrum of the UV tubes (Sylvania F15W/BLB-T8, Mass, USA) is shown in Figure 1. The degradation of stearic acid was followed by FTIR (Bruker, Coventry, UK, Vector 22). A typical stearic acid layer would have an integrated absorbance over this range of 1.0 cm^{-1} corresponding to ca. 3.13×10^{15} molecules cm^{-2} [32]. Stearic acid (100 μL of 10 mmol in methanol) was spun coated onto the sample. After drying in an oven at 55°C , the sample was exposed to UV light with an intensity of 3 mW/cm^2 . The activity of the film was defined in $\text{cm}^{-1} \text{ min}^{-1}$, which indicated the rate of reduction in selected stearic acid peaks in the IR region. The technique used was developed from work described previously [30, 32, 33].

2.2.2. Biocidal activity testing

The test used was a modification of the standard test described by BS EN 13697 : 2001. Samples were cleaned by shaking gently for 40 minutes in 40 mL of 100% methanol. Samples were removed aseptically, placed in a UVA transparent plastic Petri dish, coated side uppermost, and

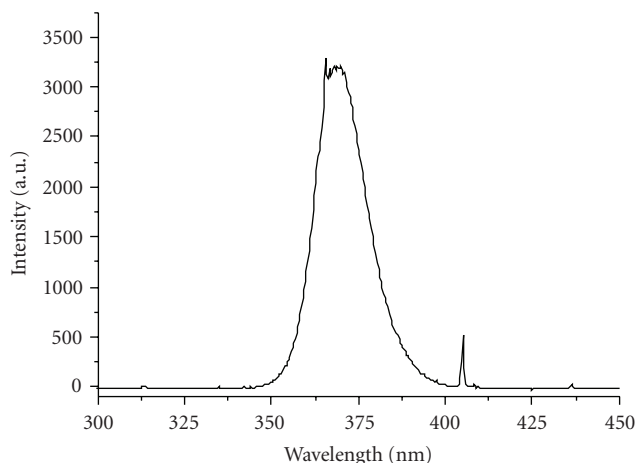


FIGURE 1: Emission spectrum of UV lamps.

preirradiated under 15 W UVA lamps (Sylvania F15W/BLB-T8) with a 2.24 mW cm^{-2} output for 24 hours.

Escherichia coli B NCIMB 9482, *E. coli* ATCC 10536, and bacteriophage T4 were obtained from the National Collection of Industrial and Marine Bacteria, Aberdeen UK, and *Staphylococcus epidermidis* NCTC11047 from the National Type Culture Collection, Colindale, UK. Bacteria were subcultured into Nutrient Broth (Oxoid, Basingstoke, UK), inoculated onto Cryobank beads (Mast Diagnostics, Liverpool, UK) and stored at -70°C . Beads were subcultured onto Nutrient Agar (Oxoid), incubated at 37°C for 24 hours and stored at 5°C . A $50 \mu\text{L}$ loopful (a plastic loop calibrated to give a defined volume) was inoculated in to 20 mL Nutrient broth (Oxoid) and incubated for 24 hours at 37°C . Cultures of *E. coli* ATCC 10536 and *S. epidermidis* were centrifuged at $5000 \times g$ for 10 minutes in a bench centrifuge, and the cells washed in deionised water $\times 3$ by centrifugation and resuspension. Controls show that this process does not affect cell viability over the test timescales. Cultures were resuspended in water and adjusted to OD 0.5 at 600 nm (Camspec, M330, Cambridge, UK) to give approximately 2×10^8 colony forming units (CFUs) mL^{-1} .

Stock bacteriophage suspension was produced by addition of bacteriophage T4 to a 24-hour culture of *E. coli* B and incubation at 37°C for a further 24 hour. Remaining cells and cell debris were removed by centrifugation at $5000 \times g$ for 10 minutes. Bacteriophage were centrifuged by centrifugation at $20\,000 \times g$ in a Sorvall RC6 centrifuge. The pellet was washed $3 \times$ by centrifugation and resuspension, plaque count determined and diluted appropriately and stored at -20°C .

Phage was assayed by the double agar layer method [34]. Phage suspension (0.1 mL) was mixed with 0.2 mL 24 hours *E. coli* B culture in nutrient broth (approx 2×10^8 CFU mL^{-1}) and 5 mL molten soft agar (Nutrient Broth + 6 g l^{-1} agar; Oxoid, UK) and poured on to surface of a nutrient agar plate. When set, the plates were incubated at 37°C for 24 hours and plaques counted.

A suspension of $50 \mu\text{L}$ of bacterial or phage was inoculated on to each test sample and spread out using the edge of a flame sterilized microscope cover slip.

The samples were UV activated by exposure to three 15 W UVA lamps (the surface incident irradiation was 2.25 mW cm^{-2} on each occasion). A sample was removed immediately and the remaining samples removed at regular intervals. Samples exposed to UVA but covered with a poly laminar UVA protection film (Anglia Window Films UK) to block UVA but not infra-red, acted as controls.

The samples were immersed in 20 mL of sterile deionised water and vortexed for 60 seconds to resuspend the organisms. A viability count was performed by serial dilution and plating onto nutrient agar in triplicate or by plaque count and incubation at 37°C for 48 hours. Each experiment was performed in triplicate.

3. RESULTS AND DISCUSSION

In order to understand the influence of the various layer structures, four types of film were produced and characterised. That of just Ag, TiO_2/Ag deposited sequentially to form layers of Ag both over and under TiO_2 and TiO_2 for reference. The two multilayered structures were deposited, so that the effect of Ag either above or below the TiO_2 layer could be assessed. The Ag films were produced with a range of thickness (60–90 nm), by increasing the number of passes of the moving substrate under the flame (see [35] for a full description of the FACVD system). The number of passes is approximately linearly related to the thickness.

3.1. Optical properties

The TiO_2 films (single and combined) were all transparent, showing interference fringes of varying colour depending on their thickness (40–120 nm). All of these films were very strongly adhered to the substrate (measured by tape pull test). Visually all the Ag films were reflective, with a pale pink tinge, which darkened to purple for thicker coatings, and eventually developed a silver appearance. The multilayered films were again reflective, those with TiO_2 grown over the Ag exhibiting accentuation of the reflected colour relating to the TiO_2 thickness. There was an increased hardness of TiO_2/Ag over Ag, which was relatively soft. (Tested by scratch resistance with a variable load traversing needle.)

3.2. Crystallinity

3.2.1. XRD

All Ag films were crystalline showing metallic cubic Ag only (JCPDS 04-0783).

Those films of Ag/TiO_2 showed no mixed species only those of Ag and TiO_2 . TiO_2 was grown directly onto the glass substrate, as expected anatase only, as discussed in a previous publication [36].

Use of Scherrer's formula [37] allows the calculation of crystallite size. The calculation is ideally for a powder not for a thin film, so will contain line width broadening from strain as well as crystallite size. Despite these reservations, the values obtained will give an idea of the changes occurring.

Considering one of the thicker Ag samples, there was an apparent increase in Ag crystallite size from 21 nm to 59 nm on addition of the TiO₂ layer. Calculations, on Ag layers covered by over-layers of TiO₂, suggest crystallite size values of 33 nm and 51 nm for anatase. The anatase value was similar to that calculated from other TiO₂ films (of similar thickness) grown under identical conditions (average 30 nm). There was no obvious change in crystallite size in TiO₂ when it is the lower layer, as expected since relatively low temperatures (300°C) were used to deposit the Ag. In previous work [35], we have shown that at higher substrate temperatures, the Ag crystallite size increases when TiO₂ overgrowth is undertaken. In this case, this most likely arises due to the high TiO₂ growth temperature (650°C), leading to annealing and growth of the Ag crystallites. As an independent check, an Ag sample was heated (650°C, 10⁰ min⁻¹) without the addition of more Ag. Although some vaporisation of the silver film appeared to have occurred, it was possible to calculate that the crystallite size still increased significantly (21 nm to 37 nm) on heating under these conditions.

Similarly, the crystallite size for Ag growth either on TiO₂ or directly on the barrier glass appeared to be equivalent in all cases, indicating that the FACVD deposition process was controlling this property.

Growth of TiO₂ layer, over the thin layer of Ag produced no changes in the Ag crystallite size. This is attributed to the relatively low-growth temperature (500°C) used for TTIP, which was probably not high enough to alter the Ag crystallite size. The anatase crystallite size was 30 nm.

3.2.2. Raman

Titania and titania underlayer samples confirmed the presence of anatase (398, 515, 636 cm⁻¹) (see Figure 2). There was an additional signal at 972 cm⁻¹ which was the only signal seen for the reference thick Ag sample. This is tentatively assigned to a plasmon resonance, which is generally defined as a coupled oscillation of conduction electrons when interacting with an external electromagnetic wave of specific wavelength. The position of the plasmon relates to the size (shape or distribution) of the Ag particles [38, 39].

3.3. Chemical composition

XPS of all the samples containing Ag confirmed this to be metallic Ag with the 3d_{5/2} peak appearing at 368.7 eV and only an O 1s signal at 533 eV relating to absorbed water and no signal for an oxide (528.2–531 eV) [40] (see Figure 2). XPS of all the samples (Ag, TiO₂, TiO₂/Ag, Ag/TiO₂) showed no major impurities in the wide scan, save the expected presence of C (standard calibration reference) and small amounts of Cl in the case of TiO₂ grown from TiCl₄ and ethyl acetate. Of major importance was the fact that both multilayer samples show signals from both TiO₂ and Ag. As XPS only samples about 5 nm of the surface, this established that the surface consists of both Ag and TiO₂.

A high resolution scan of the Ag 3d region (see Figure 3(a)) for the reference Ag film (30 passes) showed a

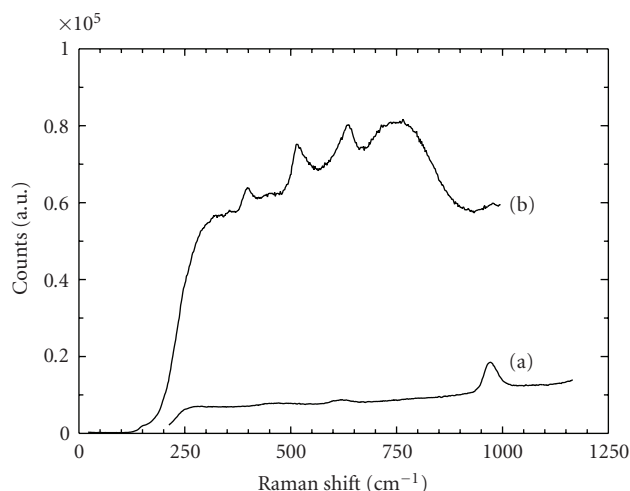


FIGURE 2: (a) Raman spectra for silver and (b) TiO₂ over silver film.

3d_{5/2} peak at 368.7 eV and a 3d_{3/2} peak at 374.7 eV, which were both shifted to lower binding energies when TiO₂ was grown on the same Ag film (3d_{5/2} = 367.9 eV and 3d_{3/2} = 373.9 eV).

The titania over Ag samples showed a slightly lower intensity of Ag (when spectra were overlaid). This is as expected, as it is partially masked by the TiO₂ layer, and in order to be located at the exposed surface of the sample the Ag atoms would have had to diffuse through the TiO₂ layer.

High resolution Ti 2p spectra (see Figure 3(b)) showing the 2p_{1/2} and 2p_{3/2} signals (464.7 eV, 459.0 eV) displayed no differences in position and width from that of a standard CVD deposited TiO₂ sample.

The O 1s (see Figure 3(c)) showed signals assigned to O bound to Ti⁴⁺ (530.2 eV) and O bound to H (532.8 eV) from absorbed water, on the lower trace. The upper trace for a thick layer of Ag (30 passes) showed only the O 1s signal for absorbed water.

From this, it can be confirmed that only Ag and TiO₂ were present. There was no shift in the positions of the Ti 2p and O 1s peaks when Ag was present, establishing that there was no significant chemical interaction of the Ag with the Ti and O. Quantitative calculation of the elements gave 1:1:2.2 ratio for Ag:Ti:O, that is, consistent with the presence of Ag metal and an oxide with the stoichiometry, TiO_{2.2}.

XPS results for Ag over TiO₂ gave very similar results to those above, confirming the presence of TiO₂ and Ag. As expected, the Ag signals were stronger as more Ag was expected to be present at the surface layer.

For Ag on top, it can be seen that the top surface contains both TiO₂ and Ag, despite the fact that they were grown as independent layers. The XPS characteristics for the multilayer of Ag on TiO₂ are readily explained on the basis that the Ag grows as nanocrystallites rather than as a continuous film. There are two possible explanations for the presence of Ag on the surface when it was originally formed as the lower layer. Either there was preferential growth of the TiO₂ on the barrier glass rather than the Ag (inhibited on Ag or faster growth on glass) or the Ag may diffuse to

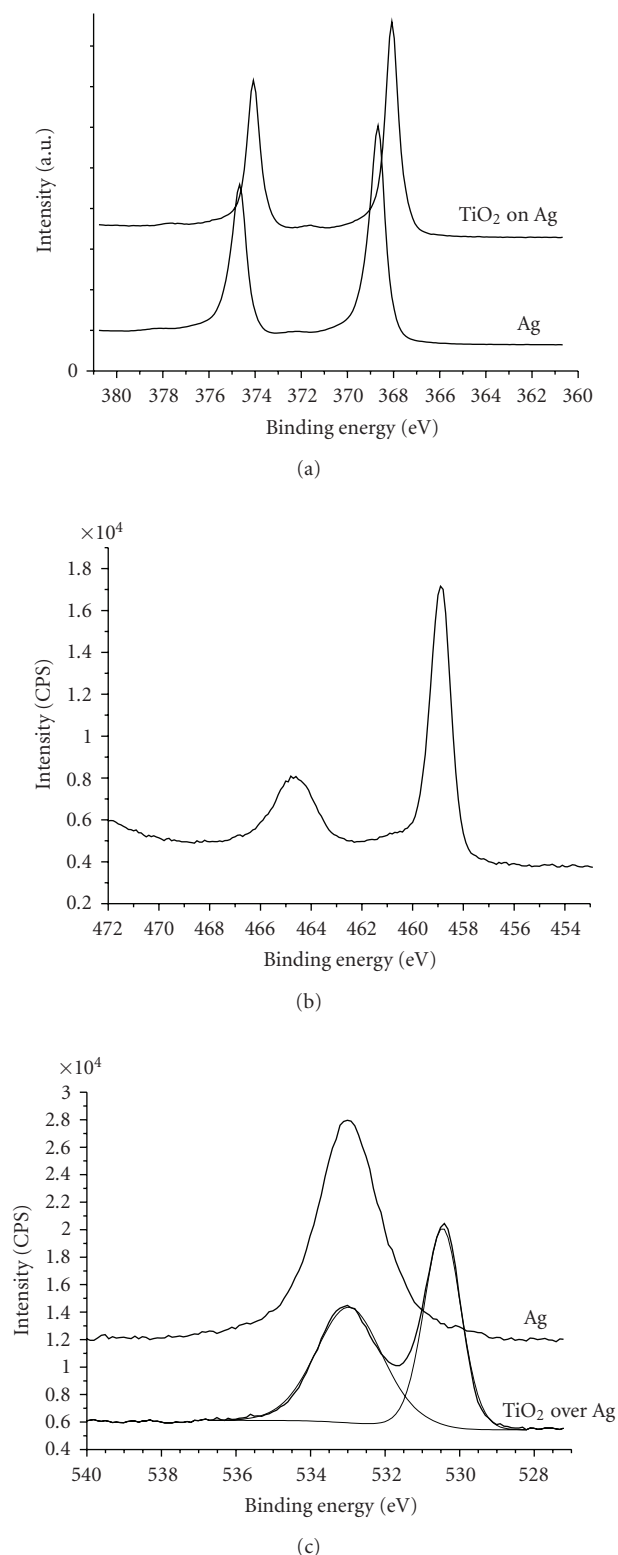


FIGURE 3: XPS high-resolution scan of (a) Ag 3d TiO₂ over Ag(30) (including sample Ag(30)), (b) Ti 2p, (c) XPS high-resolution scan for O 1s.

the surface due to the growth temperature required for TiO₂ growth.

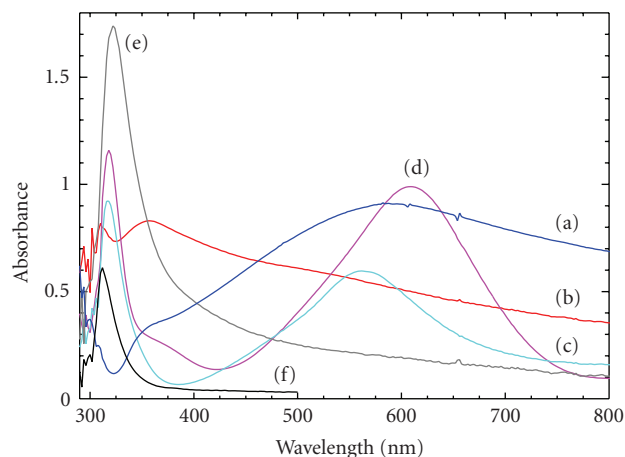


FIGURE 4: UV/Vis spectra of (a) thick layer of Ag (30 passes), (b) TiO₂ on Ag (30), (c) TiO₂ (TTIP) over Ag (4 passes), (d) Annealed TiO₂ (TTIP) over Ag (4 passes), (e) thin layer of Ag (2 passes) over TiO₂, (f) commercial TiO₂ on glass.

3.4. UV/Visible spectroscopic characteristics

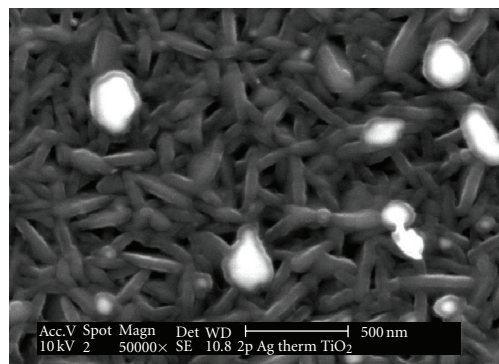
Deposition of TiO₂ on top of silver (see Figure 4(b)) showed a UV/vis absorption signal at 310 nm which relates to the TiO₂ (see trace of commercial TiO₂ on glass, Figure 4(f)). There is also a signal at 357 nm, which may be of the same origin as the shoulder seen on the Ag film with a long broad tail (see Figure 4(a)). The spectra from a sample prepared by growing a thin over-layer of Ag (2 passes) (since the silver films are not continuous, the number of passes—giving relative amount of silver deposited—is considered more valuable than a nominal approximated thickness) on TiO₂ showed only a signal relating to the TiO₂ and no sign of any Ag plasmon (see Figure 4(e)). Due to the small crystallite size (11 nm) and the lower Ag concentration, this is possibly hidden by the broad strong TiO₂ absorption band.

Spectra, for a sample prepared using TTIP as a reactant in order to deposit only anatase over Ag (4 passes), again gave absorption bands relating to both TiO₂ and an Ag plasmon (see Figure 4(c)). Interestingly on annealing this sample at 650°C, the surface plasmon shifted from 564 nm to 602 nm (see Figure 4(d)). This is in line with the expected change of wavelength as the particle size increases.

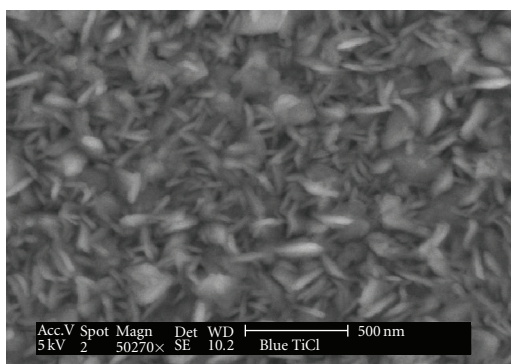
3.5. Surface structure

The FACVD process used leads to the growth of a nanostructured surface rather than a continuous Ag film. The density, size, and spacing of the nanostructured surface will depend critically on the growth conditions chosen. The image in Figure 5(a) shows growth of Ag (seen as bright particles) on top of TiO₂. Separated Ag particles between TiO₂ crystallites are readily observed.

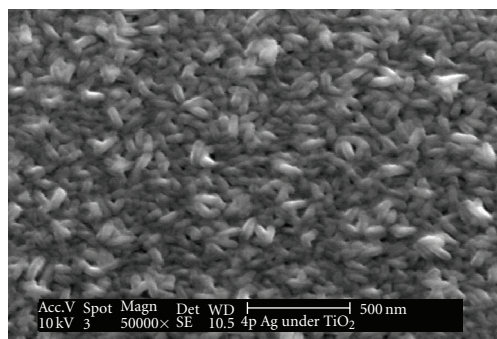
The form of the TiO₂ round and under the Ag is similar to that expected for TiO₂ grown directly on a glass substrate. The example shown in Figure 5(b) for comparison (as this is the most commonly used alternative process for CVD of



(a)



(b)



(c)

FIGURE 5: SEM images of (a) Ag(2) on top of TiO₂, (b) TiO₂ on barrier glass, (c) TiO₂ (TTIP) over Ag (4 passes).

titania) is for a TiO₂ layer grown using TiCl₄ and ethyl acetate with a thickness of ca. 120 nm.

The sample (see Figure 5(c)) with an over-layer of TiO₂ on Ag shows similar images, of the TiO₂ to that of TiO₂ grown direct on barrier glass. This is to be expected as both are only of anatase. In this instance, the SEM images look very similar, although with slightly smaller features resulting from growth on the Ag underlayer.

SEM images for TiO₂ over-layers on Ag do not show any obvious signs of Ag nanoparticles on the surface. However, use of EDAX at a series of reducing accelerating voltages (i.e., sampling closer to the surface) clearly showed that the Ag signal became stronger nearer the surface, supporting our

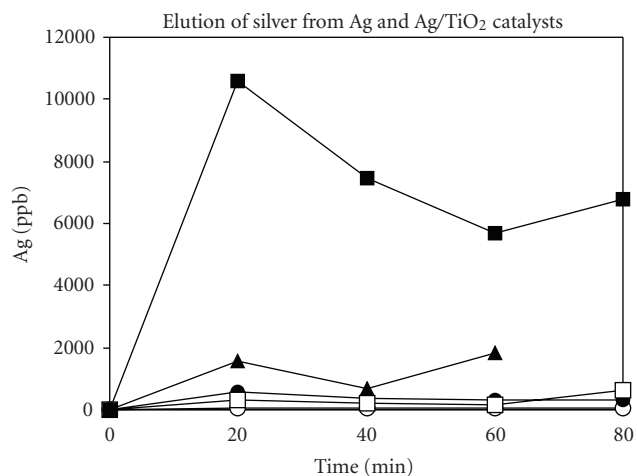


FIGURE 6: ▲ titania under, □ titania over, ■ silver only, ○ titania over with UV.

contention that at least some Ag is likely to be either exposed or very close to the surface of the sample. Unfortunately, it is not possible to accurately determine the penetration depth as this will depend on many variables including the accelerating voltage, sample matrix, and chemical identity (extent of absorption). The depth will generally vary from a few hundreds of nm to a couple of μm .

3.6. Surface Ag elution

The rate of elution of silver was tested by aqueous solution extraction-simulating the biocidal testing procedure. The sample was treated as if undergoing a bacterial test, but water and no bacteria added. After set times additional water was added, and then withdrawn, to nitric acid and the Ag content checked by ICPMS. The intention was to explore if the levels of silver eluted were sufficient to explain the biocidal activity (see Figure 6). A further objective was to assess the longevity of the bacteriocidal activity (by repeated extraction cycles). The Ag elution results are in the order silver > titania > titania under silver > titania over silver > titania only.

The concentrations of silver in the bacteria sampling solutions, for titania/silver combinations, are ~100 to 1000 ppb. For silver alone, this rises to ~10 000 ppb. It is interesting to note that silver under titania gives higher elution rates. This is compatible with the biocidal activity results.

3.7. Functional properties

3.7.1. Photoactivity

Photocatalytic activity assessment was undertaken via degradation of stearic acid under UV light (365 nm). The rate at which the stearic acid was decomposed is shown by the integrated area under the IR signals from the stearic acid (2957.5, 2922.8, and 2853.4 cm^{-1}), which are directly proportional to the concentration. The rates were obtained from the gradient of a linear (first order) fit to the raw data. As an indication of the fit error, the variance has also been given.

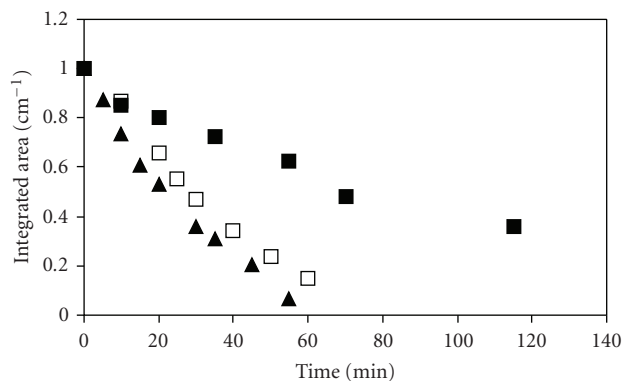


FIGURE 7: Photoactivity for the degradation of stearic acid (normalised) for ■ Ag(2), □ TiO₂ on Ag(2), ▲ TiO₂ on Ag repeat.

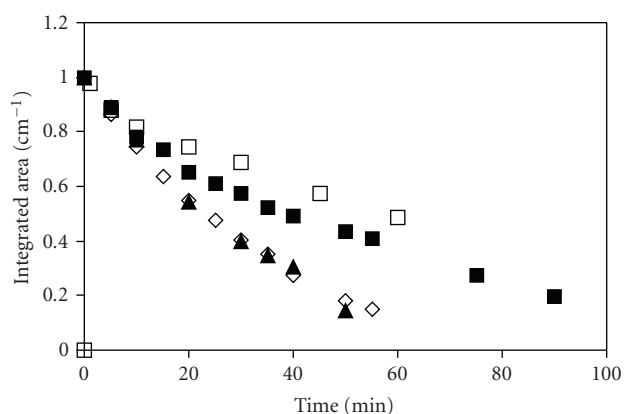


FIGURE 8: Photoactivity for the degradation of stearic acid (normalised) for Ag over TiO₂ (sample A ▲, sample B ■), reference TiO₂ ◇ and Ag on a commercial TiO₂ coating □.

This would give a value of 1 for a perfect fit. All Ag samples gave broadly similar results irrespective of the Ag deposition thickness. For example, a thick layer gave a stearic acid decomposition rate of $0.0017 \text{ cm}^{-1} \text{ min}^{-1}$ (variance 0.946) while that for a thin layer was $0.0020 \text{ cm}^{-1} \text{ min}^{-1}$ (variance 0.961). The multilayered films were UV active, although to varying degrees, depending on a range of factors.

(1) Titania over silver

TiO₂ over a thin layer of Ag (2 passes) (0.015 , $0.010 \text{ cm}^{-1} \text{ min}^{-1}$, variance 0.968) was more active than Ag and generally higher than TiO₂ alone (see Figure 7).

The comparison values for TiO₂ on barrier glass are for pure anatase. Growth of TiO₂ over Ag (4 passes) gave an activity of $0.0024 \text{ cm}^{-1} \text{ min}^{-1}$ (variance 0.974) for the combined layer, which is similar to that of just the Ag, but less than that for a single layer of TiO₂ ($0.006 \text{ cm}^{-1} \text{ min}^{-1}$, variance 0.963) of similar thickness.

The conditions of growth of TiO₂ have been shown to alter some of the physical properties of the underlying Ag (e.g., crystallite size) and so this in turn may effect the activity of the multilayer, along with the rutile/anatase ratio.

(2) Silver over titania

A thin layer of Ag (2 passes) was deposited on laboratory thermally grown TiO₂. Ag(2) on TiO₂ activity ($0.0082 \text{ cm}^{-1} \text{ min}^{-1}$, variance 0.981) (sample A in Figure 8) is referenced against TiO₂ chosen from the thickest area of the substrate before the Ag was grown. This reference should indicate the maximum activity available from anywhere on the CVD coated plate, (average $0.007 \text{ cm}^{-1} \text{ min}^{-1}$). To illustrate the effect of thickness, a second point chosen from a thinner area gives a lower activity of $0.006 \text{ cm}^{-1} \text{ min}^{-1}$ and variance of 0.940 (see Figure 8, sample B).

For comparison with commercially grown CVD titania, Ag(2) was deposited on a (uniform) commercially available (Saint-Gobain Bioclean) CVD TiO₂ coated glass giving photoactivity of $0.0054 \text{ cm}^{-1} \text{ min}^{-1}$ and variance of 0.958 (over 60 minutes) against the commercial TiO₂ coating of average $0.003 \text{ cm}^{-1} \text{ min}^{-1}$ (variance 0.976) (see Figure 8).

3.7.2. Biocidal activity

The combined thermal and FACVD grown multilayer films were investigated for biocidal activity using the bacteria *Escherichia coli* (Gram-negative), *Staphylococcus epidermidis* (Gram-positive), and bacteriophage T4.

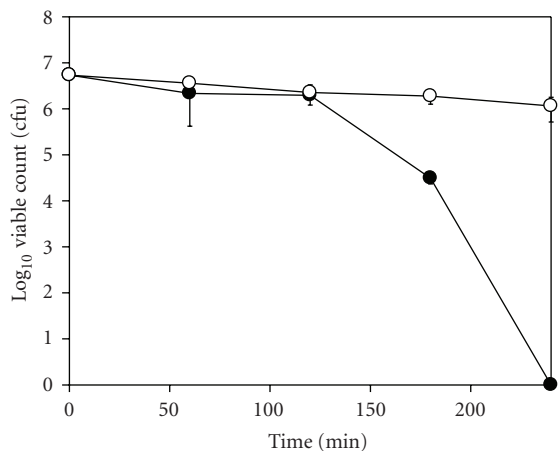
The extension of the biocidal work to Gram-positive bacteria is important because the different cell wall structure from the Gram-negative *E. coli* has been shown to decrease susceptibility to photocatalytic disinfection. The ability to disinfect viruses is also important, and bacteriophage is used as models for inactivation of mammalian viruses. There is also a large size difference between bacteria and viruses, and surface morphology may play a significant role. Plain glass was used as a control. The error bars represent the standard deviation from three separate biocidal tests. In some cases, the SD is very low and error bars are smaller than the data points. Comparisons were made between FACVD Ag layers alone, photoactive TiO₂ films, and FACVD Ag over-coated with TiO₂. All the Ag films used were about 60 nm thick (4 passes), while the comparison TiO₂ reference samples were approximately 80 nm thick.

The biocidal activity was measured by the technique outlined in Section 2. Example results (*E. coli*) are shown in Figure 9(a) for a TiO₂ layer only; see Figure 9(b) for Ag on glass and TiO₂ over Ag (see Figure 9(c)).

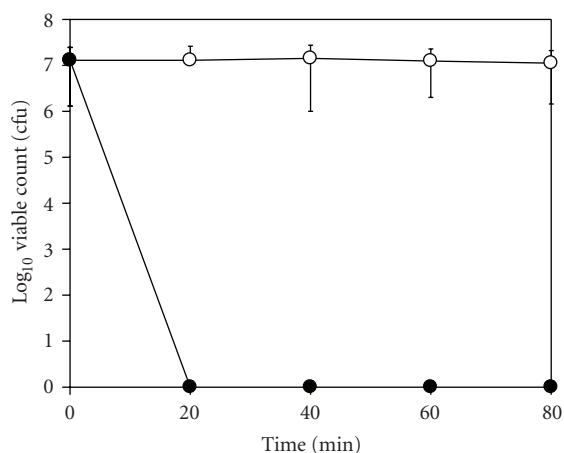
It can be seen that the thermally grown TiO₂ film was biocidally active for the Gram-negative *E. coli*, with a >5 log reduction in 180–240 minutes. All the Ag films tested were highly bacteriocidal, and most gave effectively 100% kill in under the minimum test time of 20 minutes. Although the rate of killing was slower on TiO₂ over Ag, the rate was much higher than on plain TiO₂ and these films also showed a significant enhancement of durability.

Gram-positive bacterium *Staphylococcus epidermidis* on Ag over TiO₂ was also completely killed (see Figure 10) but at a slower rate taking approx 60 minutes.

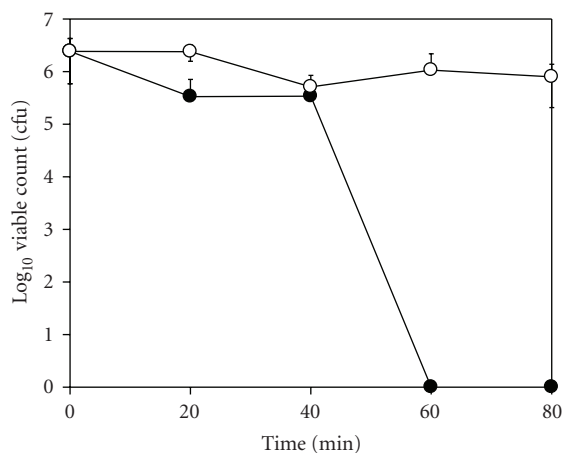
It took 80 minutes to achieve equivalent deactivation of Bacteriophage T4 (see Figure 11) on Ag over TiO₂.



(a)



(b)



(c)

FIGURE 9: (a) Killing of *E. coli* on a TiO₂ film on glass • with control sample ◦. (b) Killing of *E. coli* on Ag layer on glass (note: minimum test time 20 minutes) • with control sample ◦. (c) Killing of *E. coli* on TiO₂ layer over Ag on glass • with control sample ◦.

4. DISCUSSION

All grown films were polycrystalline, consisting of cubic Ag and TiO₂. The TiO₂ is stoichiometric anatase when the

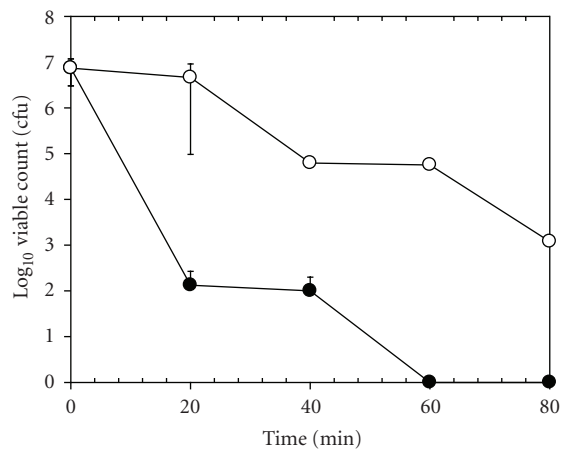


FIGURE 10: Killing of *S. epidermidis* on Ag over TiO₂.

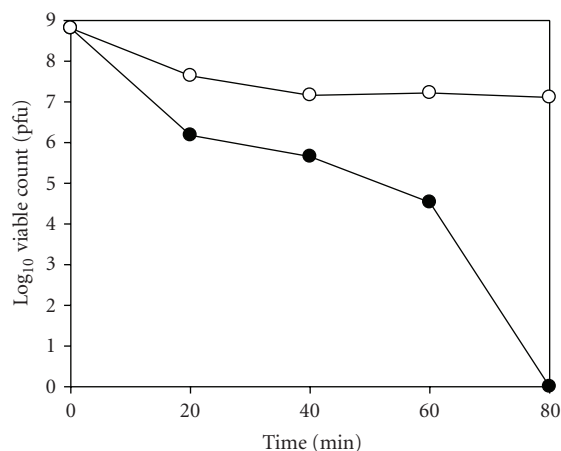


FIGURE 11: Killing of Bacteriophage T4 on Ag over TiO₂ • with control sample ◦.

bottom layer, and a mixture of anatase and rutile when over silver. XPS confirms that there is no chemical interaction between the Ag and the TiO₂. One of the interesting features of this work is that although the Ag and TiO₂ layers were grown sequentially the overall result shows that the surface consists of both Ag and TiO₂, for TiO₂ samples if the substrate temperature during growth (or after annealing post growth) is sufficiently high (> ~600C).

All the samples had some UV photoactivity, which is of differing values depending on the exact arrangement of the layers. The addition of Ag layers gives comparable or improved photoactivity of the multilayers, particularly in the case of Ag on TiO₂, over that of single layer of Ag or TiO₂ of comparable thickness.

The biocidal results show a high degree of activity for both Ag and Ag/TiO₂ films and interestingly some of the most active results are from Ag under TiO₂.

Sökmen et al. [41] used TiO₂ loaded with 1% Ag but *in suspension* and got 100% kill in 15 minutes probably due to the presence of silver ions. On TiO₂ alone, Amézaga-Madrid [9] only got a 70% reduction after 40 minutes

whereas Sunada et al. [42] saw a 6 log kill after 90 minutes with similar bacteria loadings to our own, but kill time was longer with larger doses. Kikuchi et al. [43] reported a 4-log reduction in 1 hour. Kühn et al. [44] reported a 6-log reduction of *E. coli* on P25 coated plexiglass in 1 hour. Direct comparison of biocidal activity to other data available in the literature is complicated by the different test methods used. However, it appears clear that, for thin films-based biocidal activity, the films grown in this work are highly active.

The demonstration of high activity across organisms is particularly encouraging, as Gram-positive bacteria have been shown to be more resistant [45] to photocatalytic disinfection than Gram-negative bacteria, both in suspension and on air filters [46, 47] probably due to their different cell wall structure.

Similarly, the observed high activity against bacteriophage shows that nonenveloped DNA viruses can also be inactivated and suggests that the films can be active across a wide range of organism dimensions.

The proposed mechanism for this activity is one that is strongly influenced by the thickness of the TiO₂ (80 nm). Our data suggest that this should be sufficiently thick so as to develop critical level crystallinity, but thin enough to allow silver to diffuse through (and into) the TiO₂ film as it grows. This is supported by the reported XPS results.

It should be noted that the UV levels employed in this work are of similar intensity to that found in full sunlight.

The silver elution results show that for titania/silver combinations, the level of silver in the bacteria sampling solutions was ~100 to 1000 ppb. A silver level of around 1 ppm is normally considered the minimum for significant biocidal activity. The very high levels of bactericidal activity seen with the films grown by the combination CVD process seem unlikely to be due to silver alone. Furthermore, it was observed that no killing occurred in the dark, at times up to 80 minutes, demonstrating that photocatalytic activity was crucial for high-level biocidal activity.

We can speculate that the nanostructure of Ag deposited by FACVD may be crucial in determining biocidal activity. Ag grown on glass or Ag over-coated with TiO₂, both benefit from the high-structure control capability of the FACVD approach. When deposited onto TiO₂, the structure flexibility will be, at least, partially predefined by this underlayer. Silver molecules can be oxidised at the silver/titania interface, and thus we have designed the multilayer system to incorporate a diffusion-based replenishment capability, giving the potential for extended activity. It is interesting to note that atomic absorption measurements of the bacteria solutions above the films showed concentrations below 1 ppm (Atomic Abs. detection limit).

CVD films of titania are highly durable. Indeed photocatalytic titania films made by CVD are used in commercial window "easy clean" coatings which are used on external surfaces. We have, additionally, tested our films on simulated (humidity, temperature, and exposure) and compared them to commercial samples, demonstrating close to similar performance. The titania films thus (as well as being active) also act as a host for silver.

The combination of Ag by FACVD and TiO₂, by CVD, offers unique advantages in that the CVD TiO₂ coating imparts a major enhancement to durability and as we previously have shown [29] the activity was retained along with chemical and abrasion resistance compatible with potential application of the technology. In addition, it is noteworthy that the combined Ag/TiO₂ films are thin and as such impart only moderate changes to visual appearance.

This combined flexible process along with the associated transparency and durability offers opportunity for application in the increasing number of areas where bio-active surface functionality is sought. The demonstrated capability of the films to show highly efficient biocidal activity against a range of organisms reinforces this potential.

ACKNOWLEDGMENTS

This work was partially financed by the EC through GRD1-2001-40791, PHOTOCOAT project, and partly by EPSRC. The authors acknowledge the valuable assistance of Chris Liptrot and Amran Mohammed in biocidal testing.

REFERENCES

- [1] A. Mills and S. Le Hunte, "An overview of semiconductor photocatalysis," *Journal of Photochemistry and Photobiology A*, vol. 108, no. 1, pp. 1–35, 1997.
- [2] T. Matsunaga, R. Tomoda, T. Nakajima, and H. Wake, "Photoelectrochemical sterilization of microbial cells by semiconductor powders," *FEMS Microbiology Letters*, vol. 29, no. 1-2, pp. 211–214, 1985.
- [3] P.-C. Maness, S. Smolinski, D. M. Blake, Z. Huang, E. J. Wolfrum, and W. A. Jacoby, "Bactericidal activity of photocatalytic TiO₂ reaction: toward an understanding of its killing mechanism," *Applied and Environmental Microbiology*, vol. 65, no. 9, pp. 4094–4098, 1999.
- [4] Y. Kikuchi, K. Sunada, T. Iyoda, K. Hashimoto, and A. Fujishima, "Photocatalytic bactericidal effect of TiO₂ thin films: dynamic view of the active oxygen species responsible for the effect," *Journal of Photochemistry and Photobiology A*, vol. 106, no. 1–3, pp. 51–56, 1997.
- [5] K. P. Kühn, I. F. Chaberny, K. Massholder, et al., "Disinfection of surfaces by photocatalytic oxidation with titanium dioxide and UVA light," *Chemosphere*, vol. 53, no. 1, pp. 71–77, 2003.
- [6] J. C. Yu, W. Ho, J. Lin, H. Yip, and P. K. Wong, "Photocatalytic activity, antibacterial effect, and photoinduced hydrophilicity of TiO₂ films coated on a stainless steel substrate," *Environmental Science & Technology*, vol. 37, no. 10, pp. 2296–2301, 2003.
- [7] K. Sunada, Y. Kikuchi, K. Hashimoto, and A. Fujishima, "Bactericidal and detoxification effects of TiO₂ thin film photocatalysts," *Environmental Science & Technology*, vol. 32, no. 5, pp. 726–728, 1998.
- [8] K. Sunada, T. Watanabe, and K. Hashimoto, "Bactericidal activity of copper-deposited TiO₂ thin film under weak UV light illumination," *Environmental Science & Technology*, vol. 37, no. 20, pp. 4785–4789, 2003.
- [9] P. Amézaga-Madrid, G. V. Nevárez-Moorillón, E. Orrantia-Borunda, and M. Miki-Yoshida, "Photoinduced bactericidal activity against *Pseudomonas aeruginosa* by TiO₂ based thin films," *FEMS Microbiology Letters*, vol. 211, no. 2, pp. 183–188, 2002.

- [10] Hippocrates, "On Ulcers," 400 B.C.E.; translated by Francis Adams, <http://classics.mit.edu/Browse/browse-Hippocrates.html>.
- [11] A. D. Russell and W. B. Hugo, "Antimicrobial activity and action of silver," in *Progress in Medicinal Chemistry*, G. P. Ellis and D. K. Luscombe, Eds., vol. 31, pp. 351–370, Elsevier Science, St. Louis, Mo, USA, 1994.
- [12] S. Silver, "Bacterial silver resistance: molecular biology and uses and misuses of silver compounds," *FEMS Microbiology Reviews*, vol. 27, no. 2-3, pp. 341–353, 2003.
- [13] E. Vernè, S. Di Nunzio, M. Bosetti, et al., "Surface characterization of silver-doped bioactive glass," *Biomaterials*, vol. 26, no. 25, pp. 5111–5119, 2005.
- [14] R. O. Fernández and R. A. Pizarro, "Lethal effect induced in *Pseudomonas aeruginosa* exposed to ultraviolet-a radiation," *Photochemistry and Photobiology*, vol. 64, no. 2, pp. 334–339, 1996.
- [15] K. S. Rogers, "Variable sulfhydryl activity toward silver nitrate by reduced glutathione and alcohol, glutamate and lactate dehydrogenases," *Biochimica et Biophysica Acta*, vol. 263, no. 2, pp. 309–314, 1972.
- [16] S. Y. Liau, D. C. Read, W. J. Pugh, J. R. Furr, and A. D. Russell, "Interaction of silver nitrate with readily identifiable groups: relationship to the antibacterial action of silver ions," *Letters in Applied Microbiology*, vol. 25, no. 4, pp. 279–283, 1997.
- [17] J. L. Clement and P. S. Jarrett, "Antibacterial silver," *Metal-Based Drugs*, vol. 1, no. 5-6, pp. 467–482, 1994.
- [18] R. H. Jensen and N. Davidson, "Spectrophotometric, potentiometric, and density gradient ultracentrifugation studies of the binding of silver ion by DNA," *Biopolymers*, vol. 4, no. 1, pp. 17–32, 1966.
- [19] P. D. Bragg and D. J. Rainnie, "The effect of silver ions on the respiratory chain of *Escherichia coli*," *Canadian Journal of Microbiology*, vol. 20, no. 6, pp. 883–889, 1974.
- [20] F.-R. F. Fan and A. J. Bard, "Chemical, electrochemical, gravimetric, and microscopic studies on antimicrobial silver films," *Journal of Physical Chemistry B*, vol. 106, no. 2, pp. 279–287, 2002.
- [21] S. Thomas and P. McCubbin, "A comparison of the antimicrobial effects of four silver-containing dressings on three organisms," *Journal of Wound Care*, vol. 12, no. 3, pp. 101–107, 2003.
- [22] K. Dunn and V. Edwards-Jones, "The role of Acticoat™ with nanocrystalline silver in the management of burns," *Burns*, vol. 30, supplement 1, pp. S1–S9, 2004.
- [23] C. He, Y. Yu, X. Hu, and A. Larbot, "Influence of silver doping on the photocatalytic activity of titania films," *Applied Surface Science*, vol. 200, no. 1–4, pp. 239–247, 2002.
- [24] A. Dobosz and A. Sobczyński, "The influence of silver additives on titania photoactivity in the photooxidation of phenol," *Water Research*, vol. 37, no. 7, pp. 1489–1496, 2003.
- [25] E. Stathatos, T. Petrova, and P. Lianos, "Study of the efficiency of visible-light photocatalytic degradation of basic blue adsorbed on pure and doped mesoporous titania films," *Langmuir*, vol. 17, no. 16, pp. 5025–5030, 2001.
- [26] P. D. Cozzoli, E. Fanizza, R. Comparelli, M. L. Curri, A. Agostiano, and D. Laub, "Role of metal nanoparticles in TiO₂Ag nanocomposite-based microheterogeneous photocatalysis," *Journal of Physical Chemistry B*, vol. 108, no. 28, pp. 9623–9630, 2004.
- [27] T. Hirakawa and P. V. Kamat, "Charge separation and catalytic activity of Ag-TiO₂ core-shell composite clusters under UV-irradiation," *Journal of the American Chemical Society*, vol. 127, no. 11, pp. 3928–3934, 2005.
- [28] J.-M. Herrmann, H. Tahiri, Y. Ait-Ichou, G. Lassaletta, A. R. González-Elipe, and A. Fernández, "Characterization and photocatalytic activity in aqueous medium of TiO₂ and Ag-TiO₂ coatings on quartz," *Applied Catalysis B*, vol. 13, no. 3-4, pp. 219–228, 1997.
- [29] L. A. Brook, P. Evans, H. A. Foster, et al., "Highly bioactive silver and silver/titania composite films grown by chemical vapour deposition," *Journal of Photochemistry and Photobiology A*, vol. 187, no. 1, pp. 53–63, 2007.
- [30] H. M. Yates, M. G. Nolan, D. W. Sheel, and M. E. Pemble, "Atmospheric pressure CVD growth of photocatalytic titanium dioxide thin films on tin oxide," in *Proceedings of the 15th European Conference on Chemical Vapor Deposition (EUROCV D'05)*, pp. 783–790, Electrochemical Society Proceedings, Bochum, Germany, September 2005.
- [31] M. J. Davis, G. Benito, D. W. Sheel, and M. E. Pemble, "Growth of thin films of molybdenum and tungsten oxides by combustion CVD using aqueous precursor solutions," *Chemical Vapor Deposition*, vol. 10, no. 1, pp. 29–34, 2004.
- [32] Y. Paz, Z. Luo, L. Rabenberg, and A. Heller, "Photo-oxidative self-cleaning transparent titanium dioxide films on glass," *Journal of Materials Research*, vol. 10, no. 11, pp. 2842–2848, 1995.
- [33] A. Mills, G. Hill, S. Bhopal, I. P. Parkin, and S. A. O'Neill, "Thick titanium dioxide films for semiconductor photocatalysis," *Journal of Photochemistry and Photobiology A*, vol. 160, no. 3, pp. 185–194, 2003.
- [34] A. Gratia, "Des relations numeriques entre bactéries lysogenes et particules de bactériophage," *Annales de l'Institut Pasteur*, vol. 57, pp. 652–676, 1936.
- [35] D. W. Sheel, L. A. Brook, and H. M. Yates, "Controlled nanostructured silver coated surfaces by atmospheric pressure chemical vapour deposition," *Chemical Vapor Deposition*, vol. 14, no. 1-2, pp. 14–24, 2008.
- [36] P. Evans, T. English, D. Hammond, M. E. Pemble, and D. W. Sheel, "The role of SiO₂ barrier layers in determining the structure and photocatalytic activity of TiO₂ films deposited on stainless steel," *Applied Catalysis A*, vol. 321, no. 2, pp. 140–146, 2007.
- [37] B. D. Cullity, *Elements of X-Ray Diffraction*, Addison-Wesley, Reading, Mass, USA, 1978.
- [38] T. Ung, L. M. Liz-Marzán, and P. Mulvaney, "Gold nanoparticle thin films," *Colloids and Surfaces A*, vol. 202, no. 2-3, pp. 119–126, 2002.
- [39] S. Link and M. A. El-Sayed, "Spectral properties and relaxation dynamics of surface plasmon electronic oscillations in gold and silver nanodots and nanorods," *Journal of Physical Chemistry B*, vol. 103, no. 40, pp. 8410–8426, 1999.
- [40] J. Chastain and R. C. King Jr., Eds., "Handbook of X-Ray Photoelectron Spectroscopy," Physical Electronic, Eden Prairie, Minn, USA, 1995.
- [41] M. Sökmen, F. Candan, and Z. Sümer, "Disinfection of *E. coli* by the Ag-TiO₂/UV system: lipidperoxidation," *Journal of Photochemistry and Photobiology A*, vol. 143, no. 2-3, pp. 241–244, 2001.
- [42] K. Sunada, Y. Kikuchi, K. Hashimoto, and A. Fujishima, "Bactericidal and detoxification effects of TiO₂ thin film photocatalysts," *Environmental Science & Technology*, vol. 32, no. 5, pp. 726–728, 1998.
- [43] Y. Kikuchi, K. Sunada, T. Iyoda, K. Hashimoto, and A. Fujishima, "Photocatalytic bactericidal effect of TiO₂ thin films: dynamic view of the active oxygen species responsible for the effect," *Journal of Photochemistry and Photobiology A*, vol. 106, no. 1–3, pp. 51–56, 1997.

-
- [44] K. P. Kühn, I. F. Chaberny, K. Massholder, et al., "Disinfection of surfaces by photocatalytic oxidation with titanium dioxide and UVA light," *Chemosphere*, vol. 53, no. 1, pp. 71–77, 2003.
- [45] A. Erkan, U. Bakir, and G. Karakas, "Photocatalytic microbial inactivation over Pd doped SnO₂ and TiO₂ thin films," *Journal of Photochemistry and Photobiology A*, vol. 184, no. 3, pp. 313–321, 2006.
- [46] A.-G. Rincón and C. Pulgarin, "Use of coaxial photocatalytic reactor (CAPHORE) in the TiO₂ photo-assisted treatment of mixed *E. coli* and *Bacillus* sp. and bacterial community present in wastewater," *Catalysis Today*, vol. 101, no. 3-4, pp. 331–344, 2005.
- [47] A. Pal, S. O. Pehkonen, L. E. Yu, and M. B. Ray, "Photocatalytic inactivation of Gram-positive and Gram-negative bacteria using fluorescent light," *Journal of Photochemistry and Photobiology A*, vol. 186, no. 2-3, pp. 335–341, 2007.